A drug-controllable tag for visualizing newly synthesized proteins in cells and whole animals

Michael Z. Lin*†, Jeffrey S. Glenn‡, and Roger Y. Tsien*†

*Department of Pharmacology and Howard Hughes Medical Institute, University of California at San Diego, 9500 Gilman Drive, La Jolla, CA 92093-0647; and ‡Division of Gastroenterology and Hepatology, Department of Medicine, Stanford University School of Medicine, Stanford, CA 94304-5187

Contributed by Roger Y. Tsien, March 27, 2008 (sent for review February 3, 2008)

Research on basic cellular processes involving local production or delivery of proteins, such as activity-dependent synaptic modification in neurons, would benefit greatly from a robust, nontoxic method to visualize selectively newly synthesized copies of proteins of interest within cells, tissues, or animals. We report a technique for covalent labeling of newly synthesized proteins of interest based on drug-dependent preservation of epitope tags. Epitope tags are removed from proteins of interest immediately after translation by the activity of a sequence-specific protease until the time a protease inhibitor is added, after which newly synthesized protein copies retain their tags. This method, which we call TimeSTAMP for time-specific tagging for the age measurement of proteins, allows sensitive and nonperturbative visualization and quantification of newly synthesized proteins of interest with exceptionally tight temporal control. We demonstrate applications of TimeSTAMP in retrospectively identifying growing synapses in cultured neurons and in visualizing the distribution of recently synthesized proteins in intact fly brains.

protein synthesis | protein turnover | synaptic plasticity | synaptogenesis

Spatially controlled protein production and delivery are fundamental processes in the development, maintenance, and adaptation of specialized cellular structures. Local synthesis allows for the rapid production of proteins in regions of the cell where they are needed. For example, local protein synthesis is associated with myofibril growth in cardiac myocytes (1) and contributes to actin production at the leading edge of migrating fibroblasts (2, 3). During neuronal development, guidance of axons to their targets involves the localized induction of translation in the axonal growth cone by extracellular factors (4, 5). In mature neurons, distal dendrites locally synthesize proteins in response to local stimulation by growth factors or neurotransmitters (6–8). The induction of long-term potentiation (LTP), an electrophysiological model of learning, induces the redistribution of polyribosomes to synapses and the enlargement of polyribosome-associated synapses (9, 10). Indeed, local dendritic translation is required for establishment of LTP (11). The fragile X mental retardation protein is required for stimulus-induced translation of a subset of dendritic messages, including synaptic structural elements (12, 13), implying that abnormalities in activity-dependent local synthesis of synaptic proteins may underlie some disorders of mental cognition as well.

Delivery of newly synthesized proteins to subcellular regions is also essential in maintaining specialized cellular functions. For example, sorting within the secretory pathway allows for long-distance transport of proteins from the endoplasmic reticulum to discrete final destinations within the cell. This process is necessary for the establishment and maintenance of polarized epithelial cells and of axonal and dendritic specializations in neurons, including presynaptic and postsynaptic complexes (14, 15). Local demands for particular proteins could also contribute to spatially specific protein accumulation. For example, in neurons, synapses undergoing growth could be expected to accumulate recently synthesized structural proteins from nearby pools at higher rates than stable synapses.

Studies of new protein synthesis and delivery, especially in neuronal plasticity, would benefit from the ability to visualize new proteins. However, existing methods are limited either in fidelity for reporting new proteins or compatibility with tissues or living animals. Destabilized fluorescent proteins (FPs) are used as proxy reporters of translational regulation by untranslated regions (UTRs) of mRNAs (16), but destabilized FPs are unsuitable as fusion tags of new protein localization because fusing one to a stable protein of interest would create a molecule that is more stable than the destabilized FP alone and/or less stable than the native protein of interest. In the latter case, destabilization could prevent the protein from reaching its final destination or could disrupt the function of complexes that contain the protein. Turnover of destabilized FPs is also not controllable and depends on proteasome activity, which may vary across conditions. The FP tetramer fluorescent timer slowly shifts emission over time due to fluorescence resonance energy transfer from green to red subunits as red chromophores mature (17), but it has not been used as a protein tag, likely because of its multimeric nature and uncontrollable time course. FPs that can be converted from green to red by intense short-wavelength light, such as Kaede, Eos, and Dendra, allow visual differentiation of proteins synthesized before and after photoconversion (18, 19). Similarly, fluorescence recovery after photobleaching (FRAP) allows selective visualization of newly synthesized proteins. However, photoconversion or FRAP requires uniform delivery of high-intensity UV or violet light throughout the volume of interest, which will be difficult in intact organisms and, in our experience, already causes substantial phototoxicity when applied over entire neurons. FP readouts also do not allow signal amplification and are delayed by chromophore maturation.

We have studied protein trafficking and turnover in cultured cells by sequential application of green and red biarsenical dyes (FlAsH and ReAsH) that bind to tetracysteine tags (20). However, this and similar pulse–chase chemical labeling technologies such as SNAP-tag (21) require stoichiometric binding of the first label followed by rapid washout and introduction of the second, which will be difficult at best in thick tissues and impossible in animals. Incorporation of radioactive or unnatural amino acids labels new proteins (22, 23), but nonspecifically labels all new proteins including abundant high-turnover ones and therefore cannot be used for high-resolution imaging of newly synthesized proteins of interest.

Improvements in technology are therefore necessary before visualization studies of new protein accumulation in local adaptive processes such as synaptic plasticity can be performed in the setting of an entire tissue or organism. The ideal system for visualizing newly synthesized proteins should be highly sensitive and specific for new proteins, controllable in terms of the time periods that can

Author contributions: M.Z.L. designed research; M.Z.L. performed research; M.Z.L. and J.S.G. contributed new reagents/analytic tools; M.Z.L. analyzed data; and M.Z.L. and R.Y.T. wrote the paper.

The authors declare no conflict of interest.

Freely available online through the PNAS open access option.

†To whom correspondence may be addressed. E-mail: mlin@ucsd.edu or rtsien@ucsd.edu.

This article contains supporting information online at www.pnas.org/cgi/content/full/0803060105/DCSupplemental.

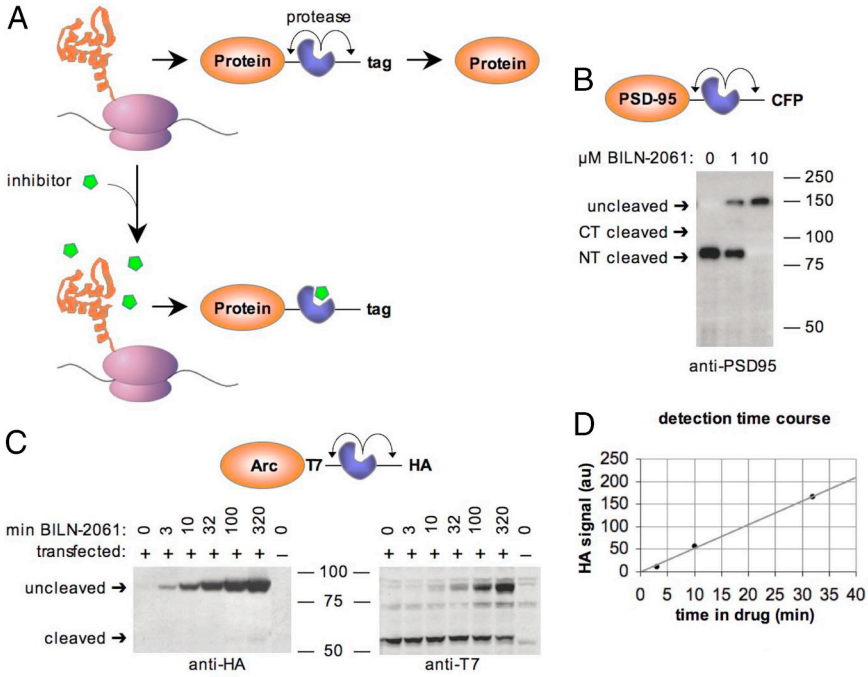

Fig. 1. TS concept and proof of concept. (*A*) Strategy for drug-dependent epitope tagging of newly synthesized proteins. (*B*) PSD-95 fused to an NS4A/B protease site, an NS3 protease domain with a T54A mutation, another NS4A/B site, and cyan fluorescent protein (CFP), is efficiently processed to release the protease and tag in the absence of the inhibitor BILN-2061. In the continual presence of BILN-2061, cleavage at both sites is efficiently inhibited. (*C*) HA tag preservation on Arc fused to the TSt cassette with N-terminal T7 and C-terminal HA tags can be detected rapidly after BILN-2061 addition (*Left*). Blotting for T7 confirms expression of the fusion protein in all conditions. (*D*) Time course of HA accumulation plotted in arbitrary units (au) vs. time after drug addition.

be investigated, applicable in whole animals, and compatible with biochemical and optical detection methods at various spatial scales. We describe a system for epitope tagging of newly synthesized proteins under the control of a cell-permeable drug that can be used in animals. In this method, an epitope tag is rapidly removed from proteins of interest by a sequence-specific protease unless a protease inhibitor is present, whereupon newly synthesized protein copies retain the tag. We call this method TimeSTAMP, for time-specific tag for the age measurement of proteins. We demonstrate the ability of TimeSTAMP (TS) to identify retrospectively new synapses in neurons based on the content of new synaptic proteins and to generate three-dimensional maps of new protein distributions in whole fly brains.

Results

Design of a Drug-Regulatable Epitope Tag. We desired to develop a tag whose presence on new proteins could be induced by the one-time administration of a small-molecule drug to either cells or animals. The strategy we devised was to incorporate a specific protease activity to confer self-removing behavior onto an epitope tag and then to use a corresponding protease inhibitor to block tag removal, so that only proteins synthesized after inhibitor application would be tagged (Fig. 1*A*). We identified the hepatitis C virus (HCV) NS3 protease as uniquely suitable for several reasons: the NS3 protease domain is small (19 kDa) and monomeric, demonstrates an unusual but well characterized substrate specificity, can be expressed in mammalian cells without noticeable toxicity, and can be specifically blocked by cell-permeant drugs developed by the pharmaceutical industry such as BILN-2061 (24–26).

We performed initial tests of our strategy in cells transfected with the model protein PSD-95 fused to combinations of various versions of NS3 protease, cognate protease sites, and tags [supporting information (SI) Fig. S1*A*]. NS3 protease lacking the NS4A cofactor efficiently and specifically cleaved at NS4A/B target sites in a manner inhibitable by BILN-2061 (Fig. S1*B*), with the best inhibition observed on a slow-cleaving NS3 variant with a Ala-54 to Thr mutation (Fig. 1*B* and Fig. S1*C*). We therefore designated a cassette comprising the NS4A/B cleavage site from the HCV polyprotein, the NS3 domain, and another NS4A/B site as the TS module, which can be fused in between a protein of interest and an epitope tag. We designate a TS module with the slow-cleaving Ala-54 NS3 variant as TSa and with the fast-cleaving Thr-54 variant as TSt. Due to its symmetric design, the TS module is suitable for tagging at either end of a protein (Fig. S1*D*). No off-target cleavage was observed in various model proteins by using either the TSa (Fig. 1 *B* and *C* and Fig. S1*D*) or TSt (Fig. S1*B*, set 4, and S1*D*) cassette.

We assessed how rapidly tag accumulation occurs after drug application. In cells expressing the activity-regulated protein Arc fused to a TS module and a distal HA tag, HA was completely removed in the absence of drug but was clearly detectable from the first time point (3 min) after drug application (Fig. 1*C*). A T7 epitope tag placed proximal to the cleavage sites showed that the protein was expressed at all times (Fig. 1*C*). Initial accumulation of HA-tagged protein followed a linear relationship ($R = 0.997$), as expected given a constant rate of production (Fig. 1*D*). The ability to detect tag accumulation within 3 min of drug application demonstrates that the TS strategy allows control of tag preservation with high temporal resolution.

We tested the ability of TS to tag new proteins in primary hippocampal neurons. Cultured neurons expressing PSD-95-GFP fused to TSa and a C-terminal HA tag (PSD-95-GFP-TSa-HA) showed punctate HA immunofluorescence (IF) in the presence of BILN-2061 but not in its absence (Fig. 2*A*). No HA staining was observed in transfected neurons in the absence of drug, demonstrating that cleaved tag degrades rapidly and/or is lost during fixation (Fig. 2*A*). Similar results were obtained with TSa fusions to synaptic proteins Arc and Neuroligin1 (Fig. S2*A*). To recapitulate endogenous mechanisms of mRNA regulation, the 5′ and 3′ UTRs were included in all constructs. As expected, the protein synthesis inhibitor cycloheximide prevented HA signal accumulation (Fig.

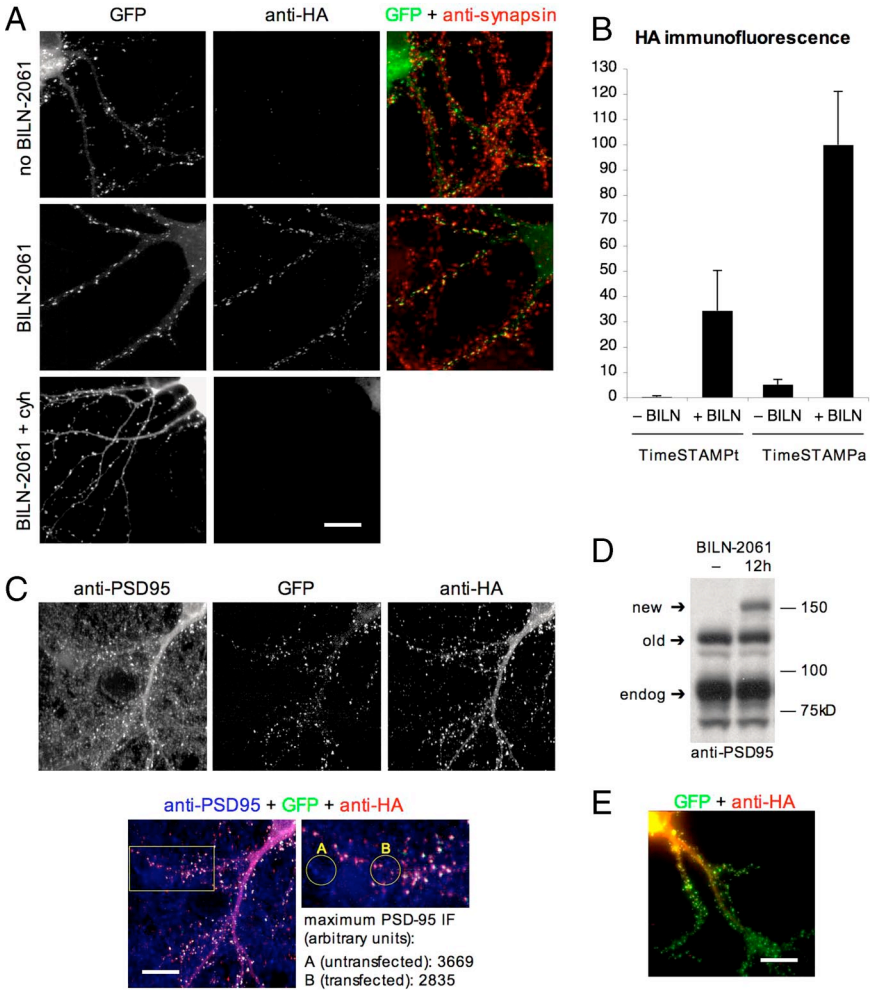

Fig. 2. TS allows selective and sensitive labeling of new PSD-95 in neurons. (*A*) TS-mediated IF is specific for new proteins. Eighteen days *in vitro* (DIV) neurons at 9 days posttransfection (DPT) with PSD-95-GFP-TSa-HA show synaptic HA IF after 6 h of BILN-2061. Staining is absent without BILN-2061 or when protein synthesis is blocked by 50 μg/ml cycloheximide (cyh). (*B*) Quantitative HA IF of 18 DIV neurons at 9 DPT shows mean contrast of 121-fold for PSD-95-TSt and 20-fold for PSD-95-TSa, with TSa demonstrating higher levels. Data represent mean ± SEM. (*C*) To assess limits of detection, 21 DIV neurons at 11 DPT were stained for PSD-95 and HA after 6 h of BILN-2061. Measurement of maximum PSD-95 IF in untransfected or transfected neurites shows HA staining of PSD-95 at levels within the endogenous range. (*D*) In 21 DIV neurons at 21 DPT, 22% of total transfected PSD-95 was synthesized in 12 h, consistent with native PSD-95 turnover rates. (*E*) TS reports spatial distributions of new proteins. After 6 h in BILN-2061, a gradient of newly synthesized PSD-95 from the cell soma can be seen. (Scale bars, 20 μm.) Maximum intensity projections of confocal (*A* and *C*) or epifluorescence images (*E*) spaced 0.5 μm through the neuron are shown.

2*A*), whereas brain-derived neurotrophic factor, which induces Arc translation in neurons (27), increased accumulation of Arc-TSa-HA (Fig. S2*B*). Drug induced a 20-fold increase in signal with TSa and a 121-fold increase with TSt (Fig. 2*B*). HA staining detected newly synthesized PSD-95-GFP-TSa-HA at levels comparable with endogenous PSD-95 (Fig. 2*C*). Thus, TS is specific, sensitive, and generalizable.

We asked whether TS tagging might perturb protein behavior or be toxic. PSD-95-GFP-TSa-HA was present in dendrites and enriched in puncta in dendritic spines, indicating proper localization (Fig. 2*A*). TS tagging did not significantly affect protein turnover because replacement rates of PSD-95-GFP-TSa-HA in stably transfected neurons were consistent with the previously measured 36-h half-life of endogenous PSD-95 (Fig. 2*D*) (28). We observed no abnormalities in neuronal morphology or synaptic density after expression throughout synaptogenesis of PSD-95 fused to TSa or TSt modules (Fig. S2*C*, constructs 4, 6, and 7). Test constructs containing the more active wild-type NS3 domain fused permanently to PSD-95 resulted in lower synaptic densities (Fig. S2*C*, constructs 1 and 3), but this effect could be rescued by either allowing protease self-release from PSD-95 (Fig. S2*C*, construct 2), as occurs in the TS modules, or introduction of the T54A mutation (Fig. S2*C*, construct 5). These experiments demonstrate that the use of TS modules to label proteins is nonpertubative and nontoxic.

We investigated whether TS can report the spatial distribution of new proteins. In neurons expressing PSD-95-GFP-TSa-HA treated with BILN-2061 for 6 h, a time in which ≈11% of PSD-95 molecules will turn over, assuming steady-state expression and a 36-h half-life, we observed gradients of new protein down the dendrites, distinct from total PSD-95-GFP, which was distributed throughout the cell (Fig. 2*E*). Likewise, we observed new Neuroligin1 predominantly in the soma after 6 h, distinct from total Neuroligin1 (Fig. S2*D*), consistent with processing in the secretory pathway. To verify these findings by using another method, we expressed PSD-95 or Neuroligin1 fused to tandem dimer EosFP, which converts from green to red emission upon near-UV irradiation (19). After photoconversion of existing protein into red fluorescence, new protein appears green. Although photoconversion causes death of some neurons, it allowed us to confirm in surviving neurons that newly synthesized PSD-95 and Neuroligin1 exist in a gradient from the soma (Fig. S3). These results show that the TS method can report distributions of newly synthesized proteins.

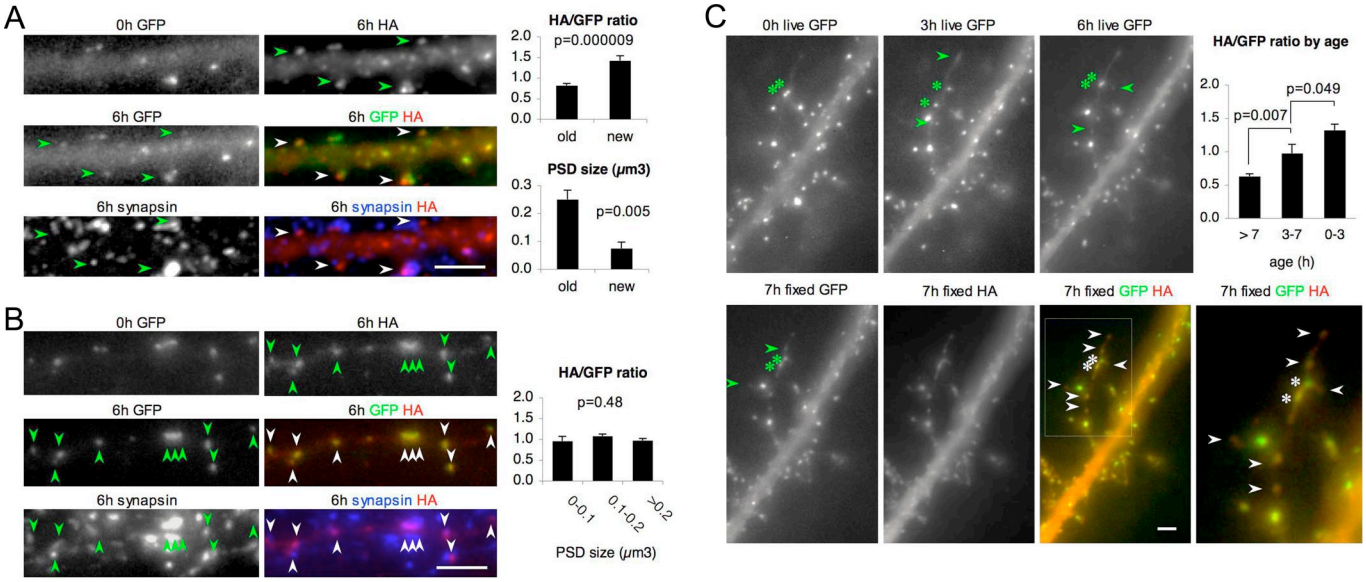

Fig. 3. Newly forming synapses preferentially accumulate new PSD-95. (*A*) Twenty-one days *in vitro* neurons at 14 DPT expressing PSD-95-GFP-TSa-HA were imaged at the time of BILN-2061 addition. After fixation 6 h later, cells were stained for HA for newly synthesized PSD-95 and synapsin to verify the synaptic identity of PSD-95 puncta. Arrowheads mark synapses appearing during the experiment. New synapses show significantly higher HA/GFP intensity ratios and smaller size. (*B*) Stable synapses of different sizes (arrowheads) show similar HA/GFP ratios. (*C*) Synaptic nascence correlates with the new PSD-95 fraction. Fourteen days *in vitro* neurons at 7 DPT were treated with BILN-2061 while GFP puncta formation was tracked by time-lapse microscopy, then neurons were stained for HA. Newly appearing puncta are marked by arrowheads. Asterisks track two preexisting mobile puncta. HA/GFP ratios of synapses are inversely correlated with their age ($n = 27$). For all panels, data represent mean ± SEM. HA/GFP ratios are in arbitrary units normalized to population mean. Maximal intensity projections of epifluorescence images spaced 0.5 μm through the neuron are shown. (Scale bars, 5 μm.)

Application of TS to Tracking Synaptic Growth. Growth or *de novo* formation of synapses occurs in response to circuit activity or biochemical stimulation and may underlie some forms of learning (9, 29–31). Determining where synapses are growing is therefore critical in understanding circuitry adaptation. Although time-lapse microscopy can track synaptic growth in sparsely labeled neurons in superficial brain regions (32), visualizing growth in deep regions or during unrestrained behavior has not been possible. A plausible strategy may be to image new protein accumulation by growing synapses. A large body of evidence suggests that PSD-95 accumulates in growing synapses from a diffuse cytoplasmic pool (33). Furthermore, based on local photoactivation and FRAP experiments, spines in differentiating hippocampal neurons appear to contain two populations of PSD-95 molecules, with 25–40% of PSD-95 protein exchanging with a half-time of minutes and the remainder relatively immobile on the order of hours (34–36).

We explored the possibility of using TS on synaptic proteins to assess synaptic growth retrospectively over a few hours. We acquired GFP images of neurons expressing PSD-95-GFP-TSa-HA during synaptic differentiation in the presence of BILN-2061 for 6 h, a time interval appropriate for detecting the formation of several synapses per microscope field (37). Comparing GFP images from the beginning and the end, we identified new postsynaptic densities (PSDs) as newly appearing PSD-95-GFP puncta that colocalized with the presynaptic marker synapsin. These new PSDs showed significantly higher HA IF relative to GFP, indicating that they preferentially incorporate new PSD-95 (Fig. 3*A*). New PSDs were also smaller on average (Fig. 3*A*), but small size alone is not a sufficient indicator of new synapses because some neurons exhibited small PSDs at the end of the experiment that existed before the observation period (Fig. 3*B*). These stable small PSDs also had HA/GFP ratios similar to those of nearby stable large PSDs (Fig. 3*B*), demonstrating that larger PSDs do not inherently demonstrate lower HA/GFP ratios, e.g., because of incomplete antibody access. These results show that a high fractional content of new PSD-95 characterizes recently formed synapses. Using 3-h intervals, we confirmed that the HA/GFP ratio was correlated with PSD newness, so that more recently appearing PSD had significantly higher HA/GFP ratios than those appearing earlier (Fig. 3*C*), further supporting this relationship and demonstrating that differences in new PSD-95 content arise within 3 h. In all of our experiments, we observed that old PSDs maintained distinctly lower HA/GFP ratios than the adjacent dendritic shaft, confirming that synaptic PSD-95 molecules are not in complete rapid exchange with the PSD-95 pool in the dendritic shaft. Taken together, these results show that visualization of newly synthesized proteins by TS can be used to identify nascent synapses retrospectively in differentiating neurons.

Whole-Brain Mapping of New Protein Distributions in Living Animals. The ability of TS to be controlled by a cell-permeable drug should allow time-specific protein tagging in a living animal. The fruit fly *Drosophila melanogaster* has emerged as a preeminent model for studying neuronal circuitry (38). We chose to examine fly calcium/calmodulin-dependent protein kinase II (dCaMKII), whose transcription occurs throughout the nervous system (39) but whose translation and synaptic localization are influenced by neuronal activity (40). We asked whether TS could be used to generate a three-dimensional map of new dCaMKII protein to reveal whether new dCaMKII distributions vary between or within neurons of the fly brain. Because the dCaMKII C terminus mediates homododecamerization, we tagged dCaMKII at the N terminus by using a TSt module in which an HSV tag serves as the a drug-dependent epitope and a HA tag as a constitutive epitope. This HSV-TSt-HA-dCaMKII fusion protein demonstrates BILN-2061-dependent HSV tag preservation in transfected cells at the ambient temperatures in which flies are raised (Fig. S1*D*). We then created transgenic fly lines expressing HSV-TSt-HA-dCaMKII under the control of the elav promoter, which drives expression in all neurons with enrichment in the mushroom bodies (MBs), a pattern similar to endogenous dCaMKII protein (39). We administered BILN-2061 for 6 h to living flies, then we stained and visualized HSV-tagged new and HA-tagged total protein by confocal microscopy.

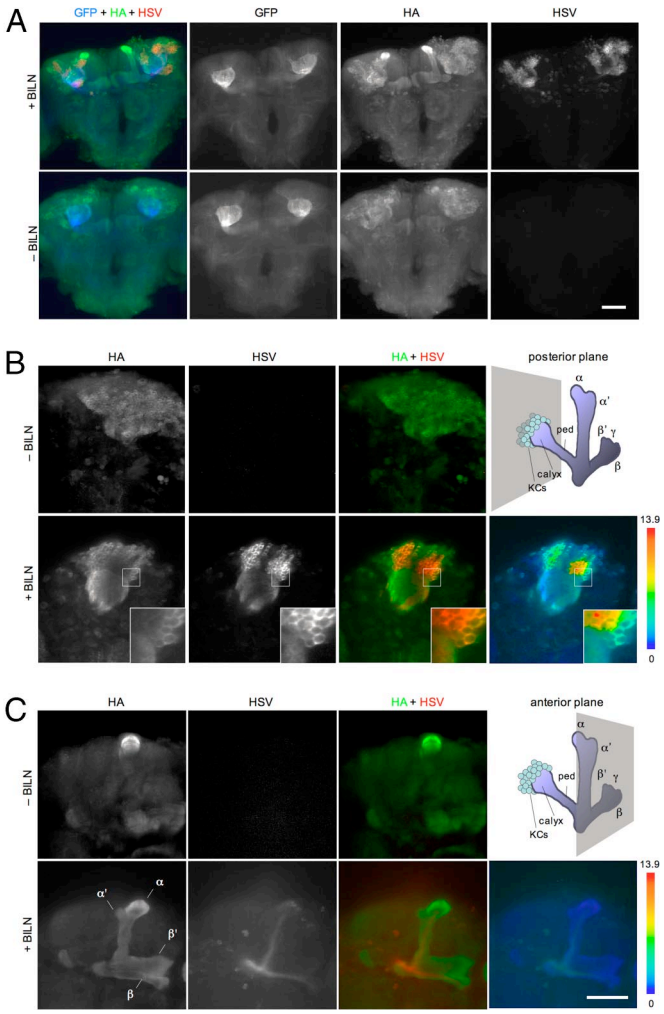

Fig. 4. TS tagging of newly synthesized proteins in whole flies. (*A*) Adult flies expressing HSV-TSt-HA-dCaMKII and tubulin-GFP in neurons were administered BILN-2061 for 6 h, then brains were stained. HSV IF reveals distributions of newly synthesized dCaMKII, whereas HA IF reveals total dCaMKII. No HSV IF is observed in flies not administered BILN-2061. (*B*) Kenyon cells are heterogeneous in dCaMKII production. (*Inset*) Enlarged image of the boxed area. (*Upper Right*) Diagram of the right MB. ped, peduncle. (*Right*) A HSV/HA ratiometric image reveals sites of relative enrichment of new dCaMKII. The HSV/HA ratio is represented in pseudocolor intensity-modulated display, scaled in arbitrary units relative to the mean whole-brain HSV/HA ratio. (*C*) New dCaMKII is present in α and β lobes, but not α', β', or γ lobes, at lower levels than in cell bodies. Anti-HSV intensity is scaled 4-fold higher than in *B* for visibility, otherwise parameters are identical. Maximum intensity projections of confocal sections spaced 5 μm apart throughout the fly brain *A* or of two adjacent sections (*B* and *C*) are shown. (Scale bars, 20 μm.)

HA revealed that total HSV-TSt-HA-dCaMKII protein was expressed throughout brains with enrichment in the MBs, similar to elav-driven tubulin-GFP (Fig. 4*A*). As expected, HSV IF was observed only in the presence of inhibitor (Fig. 4*A*).

New dCaMKII was particularly abundant in scattered neurons in the anterior protocerebrum near the MB lobes and in groups of Kenyon cells (KCs) of the MB (Fig. 4*A* and Fig. S4*A*). KCs project axons through the peduncles that then branch in the α, α', β, β', and γ lobes of the MBs. High levels of new dCaMKII could be traced from the KC soma along discrete axonal bundles continuous with moderate levels of new dCaMKII in the α and β lobes (Fig. 4 *B* and *C* and Fig. S4*A*). In contrast, no HSV IF was observed in the α', β', and γ lobes, even though total dCaMKII protein, as revealed by HA IF, is equally abundant in the α, α', β, β', and γ lobes (Fig. 4*C*). These results indicate that KCs projecting to the α and β lobes maintain higher rates of dCaMKII synthesis than KCs projecting to the α', β', and γ lobes. Interestingly, α/β KCs represent a developmentally and functionally distinct population of KCs (41, 42).

TS tagging also revealed subcellular differences in new protein distributions. Within KCs, HSV intensities and HSV/HA ratios are complementary to total dCaMKII, with higher levels in the cell bodies and peduncle than in the distal axon branches (Fig. 4). This pattern of dCaMKII turnover is consistent with dCaMKII production in the KCs occurring predominantly in soma. Similar results were obtained in flies expressing the slower cleaving HSV-TSa-HA-dCaMKII (Fig. S4*B*). Taken together, these results show that the TS technique reveals heterogeneity in dCaMKII production between neurons and in the subcellular distribution of new dCaMKII molecules in the brains of living animals.

Discussion

By tightly linking onset of protein tagging to the presence of a drug, the TS method allows temporally controlled labeling of newly synthesized proteins of interest in thick tissues or intact animals. We have demonstrated that TS is sensitive, specific, nonperturbing, nontoxic, and generalizable. Taking advantage of these attributes, we have demonstrated that growing synapses in primary neurons preferentially accumulate new PSD-95 molecules. We have also visualized the distribution of newly synthesized dCaMKII throughout the fly brain, demonstrating that TS can be used to label proteins synthesized during unrestrained behavior in animals.

In addition to its unique ability to control protein tagging *in vivo*, TS combines the temporal resolution of small-molecule regulation and the high sensitivity and specificity of antibodies, and it may be the method of choice in some *in cellulo* situations as well. Signal can be detected within minutes of drug addition, a time resolution finer than sequential chemical labeling with its long incubation and wash times. The sensitivity of antibody staining, where signal amplification can be achieved with secondary antibodies, allows the visualization of even low-abundance proteins. For example, synaptic proteins such as PSD-95 are present at a few hundred copies per synapse (43, 44), only a fraction of which will be synthesized within a few hours. In contrast, signals from photoconvertible proteins cannot be further amplified, are limited by photobleaching of converted protein, and are delayed by chromophore maturation.

TS should be adaptable to other antibody-based detection methods. For example, immunoelectron microscopy could be performed to reveal new proteins at the synapse with ultrastructural resolution. The TS method also allows multiplexing; unique epitope tags on different proteins of interest can be detected with antibodies conjugated to different fluorophores for fluorescence microscopy or to differently sized quantum dots for correlated fluorescence and electron microscopy (45). We have already demonstrated TS in immunoblotting, where it allows quantitation of proteins produced before vs. after a time of interest. It has also not escaped our attention that highly specific protease–inhibitor pairs could be used to regulate the attachment of functional peptide motifs, not just epitope tags, and work is needed to explore these possibilities.

Our results with PSD-95 also provide proof of concept for an approach to identifying synapses undergoing growth within the intact brain in response to environmental changes, learning, or pathway stimulation. Although we have focused on postsynaptic proteins, presynaptic proteins will also be of interest. Other proteins may be more immobile or turn over more slowly in stable synapses than PSD-95. As candidates are identified, it will be of interest to test their ability to serve as reporters of synaptic growth.

Materials and Methods

Construction and Initial Testing of TS. HCV genotype 1a NS4A and NS3 coding sequences were obtained by RT-PCR from infected macaque liver RNA. The HCV NS3 protease inhibitor BILN-2061 was custom-synthesized by Acme Bio-

sciences. For initial tests by immunoblotting, linear fusions of PSD-95, the HCV NS3 protease domain lacking the helicase domain flanked on both sides by cleavage sites, an HA epitope tag, and the CFP were constructed. The NS4A β strand, which enhances NS3 protease activity *in trans* (46), was either fused N-terminal to the NS3 domain, a configuration shown to possess high catalytic activity (47), or omitted. In some constructs and in the final TSa cassette, we introduced a mutation of Thr-54 to Ala that had been found to reduce the catalytic rate of the enzyme 10-fold (48). Analysis of the protease structure (49) revealed Thr-54 to be distant from the catalytic triad and the BILN-2061 binding site. Rather, Thr-54 may help shape the oxyanion hole; its hydrogen bond with the backbone oxygen of Leu-44 may help orient the Leu-44 side chain, which in turn interacts with the peptide backbone of the oxyanion hole. For cleavage sites, we chose the NS4A/4B junction because it is efficiently cleaved by NS3 protease and because the NS4A cleavage product can bind to the active site and competitively inhibit the protease with an inhibitory constant of 0.6 μM (50), possibly limiting further protease activity. Fusions using cleavage sites from the NS5A/5B junction showed reduced sensitivity to inhibition by BILN-2061 (data not shown), consistent with the faster activity of NS3 protease on this sequence (51). We also created for comparison constructs without a cleavage site in between PSD-95 and the protease domain. HEK293 cells were transfected by using Lipofectamine 2000, then grown for 2 days with or without BILN-2061. SDS lysates were prepared, followed by SDS/PAGE and immunoblotting with anti-PSD-95 to differentiate uncleaved and cleaved products by size. Constructs containing the NS4A β strand were inefficiently inhibited by BILN-2061 in early experiments and were not explored further.

Neuronal and Fly Materials and Methods. See *SI Materials and Methods*.

ACKNOWLEDGMENTS. We thank Michael McKeown, Holli Weld, and Evangeline Mose for assistance with experiments; Paul Steinbach with microscopy, Stefan Wieland and Frank Chisari (Scripps Research Institute, La Jolla, CA) for liver RNA from HCV-infected macaques, Joerg Wiedenmann (University of Ulm) for EosFP cDNA, Cynthia Hughes, Marco Gallo, Jing Wang, and Charles Zuker (University of California, San Diego, CA) for fly stocks and advice, Terunaga Nakagawa for discussion, and members of the Tsien and Glenn laboratories for their support. This work was supported by a Jane Coffin Childs fellowship (to M.Z.L.), by the Howard Hughes Medical Institute and National Institutes of Health (to R.Y.T.), and by a Burroughs Wellcome Fund Clinical Scientist Award in Translational Research and National Institutes of Health (to J.S.G.).

1. Larsen TH, Saetersdal T (1998) Translocation of 60S ribosomal subunit in spreading cardiac myocytes. *J Histochem Cytochem* 46:963–970.
2. Huttelmaier S, *et al.* (2005) Spatial regulation of β-actin translation by Src-dependent phosphorylation of ZBP1. *Nature* 438:512–515.
3. Rodriguez AJ, Shenoy SM, Singer RH, Condeelis J (2006) Visualization of mRNA translation in living cells. *J Cell Biol* 175:67–76.
4. Leung KM, *et al.* (2006) Asymmetrical β-actin mRNA translation in growth cones mediates attractive turning to netrin-1. *Nat Neurosci* 9:1247–1256.
5. Wu KY, *et al.* (2005) Local translation of RhoA regulates growth cone collapse. *Nature* 436:1020–1024.
6. Bramham CR, Wells DG (2007) Dendritic mRNA: Transport, translation and function. *Nat Rev Neurosci* 8:776–789.
7. Steward O, Schuman EM (2003) Compartmentalized synthesis and degradation of proteins in neurons. *Neuron* 40:347–359.
8. Sutton MA, Schuman EM (2006) Dendritic protein synthesis, synaptic plasticity, and memory. *Cell* 127:49–58.
9. Harris KM, Fiala JC, Ostroff L (2003) Structural changes at dendritic spine synapses during long-term potentiation. *Philos Trans R Soc London Ser B* 358:745–748.
10. Ostroff LE, Fiala JC, Allwardt B, Harris KM (2002) Polyribosomes redistribute from dendritic shafts into spines with enlarged synapses during LTP in developing rat hippocampal slices. *Neuron* 35:535–545.
11. Bradshaw KD, Emptage NJ, Bliss TV (2003) A role for dendritic protein synthesis in hippocampal late LTP. *Eur J Neurosci* 18:3150–3152.
12. Muddashetty RS, Kelic S, Gross C, Xu M, Bassell GJ (2007) Dysregulated metabotropic glutamate receptor-dependent translation of AMPA receptor and postsynaptic density-95 mRNAs at synapses in a mouse model of fragile X syndrome. *J Neurosci* 27:5338–5348.
13. Zalfa F, *et al.* (2007) A new function for the fragile X mental retardation protein in regulation of PSD-95 mRNA stability. *Nat Neurosci* 10:578–587.
14. Muth TR, Caplan MJ (2003) Transport protein trafficking in polarized cells. *Annu Rev Cell Dev Biol* 19:333–366.
15. Horton AC, *et al.* (2005) Polarized secretory trafficking directs cargo for asymmetric dendrite growth and morphogenesis. *Neuron* 48:757–771.
16. Aakalu G, Smith WB, Nguyen N, Jiang C, Schuman EM (2001) Dynamic visualization of local protein synthesis in hippocampal neurons. *Neuron* 30:489–502.
17. Verkhusha VV, Chudakov DM, Gurskaya NG, Lukyanov S, Lukyanov KA (2004) Common pathway for the red chromophore formation in fluorescent proteins and chromoproteins. *Chem Biol* 11:845–854.
18. Raab-Graham KF, Haddick PC, Jan YN, Jan LY (2006) Activity- and mTOR-dependent suppression of Kv1.1 channel mRNA translation in dendrites. *Science* 314:144–148.
19. Wiedenmann J, *et al.* (2004) EosFP, a fluorescent marker protein with UV-inducible green-to-red fluorescence conversion. *Proc Natl Acad Sci USA* 101:15905–15910.
20. Ju W, *et al.* (2004) Activity-dependent regulation of dendritic synthesis and trafficking of AMPA receptors. *Nat Neurosci* 7:244–253.
21. O'Hare HM, Johnsson K, Gautier A (2007) Chemical probes shed light on protein function. *Curr Opin Struct Biol* 17:488–494.
22. Beatty KE, *et al.* (2006) Fluorescence visualization of newly synthesized proteins in mammalian cells. *Angew Chem Int Ed Engl* 45:7364–7367.
23. Dieterich DC, Link AJ, Graumann J, Tirrell DA, Schuman EM (2006) Selective identification of newly synthesized proteins in mammalian cells using bioorthogonal noncanonical amino acid tagging (BONCAT). *Proc Natl Acad Sci USA* 103:9482–9487.
24. Bartenschlager R (1999) The NS3/4A proteinase of the hepatitis C virus: Unravelling structure and function of an unusual enzyme and a prime target for antiviral therapy. *J Viral Hepatol* 6:165–181.
25. Thomson JA, Perni RB (2006) Hepatitis C virus NS3–4A protease inhibitors: Countering viral subversion *in vitro* and showing promise in the clinic. *Curr Opin Drug Discov Dev* 9:606–617.
26. Lamarre D, *et al.* (2003) An NS3 protease inhibitor with antiviral effects in humans infected with hepatitis C virus. *Nature* 426:186–189.
27. Yin Y, Edelman GM, Vanderklish PW (2002) The brain-derived neurotrophic factor enhances synthesis of Arc in synaptoneurosomes. *Proc Natl Acad Sci USA* 99:2368–2373.
28. El-Husseini A-D, *et al.* (2002) Synaptic strength regulated by palmitate cycling on PSD-95. *Cell* 108:849–863.
29. Kopec CD, Li B, Wei W, Boehm J, Malinow R (2006) Glutamate receptor exocytosis and spine enlargement during chemically induced long-term potentiation. *J Neurosci* 26:2000–2009.
30. Matsuzaki M, Honkura N, Ellis-Davies GC, Kasai H (2004) Structural basis of long-term potentiation in single dendritic spines. *Nature* 429:761–766.
31. Nagerl UV, Eberhorn N, Cambridge SB, Bonhoeffer T (2004) Bidirectional activity-dependent morphological plasticity in hippocampal neurons. *Neuron* 44:759–767.
32. Trachtenberg JT, *et al.* (2002) Long-term *in vivo* imaging of experience-dependent synaptic plasticity in adult cortex. *Nature* 420:788–794.
33. Li Z, Sheng M (2003) Some assembly required: The development of neuronal synapses. *Nat Rev Mol Cell Biol* 4:833–841.
34. Nakagawa T, *et al.* (2004) Quaternary structure, protein dynamics, and synaptic function of SAP97 controlled by L27 domain interactions. *Neuron* 44:453–467.
35. Sharma K, Fong DK, Craig AM (2006) Postsynaptic protein mobility in dendritic spines: Long-term regulation by synaptic NMDA receptor activation. *Mol Cell Neurosci* 31:702–712.
36. Xu W, *et al.* (2008) Molecular dissociation of the role of PSD-95 in regulating synaptic strength and LTD. *Neuron* 57:248–262.
37. Friedman HV, Bresler T, Garner CC, Ziv NE (2000) Assembly of new individual excitatory synapses: Time course and temporal order of molecule recruitment. *Neuron* 27:57–69.
38. Desplan C (2007) Time to pick the fly's brain. *Nature* 450:173.
39. Takamatsu Y, Kishimoto Y, Ohsako S (2003) Immunohistochemical study of Ca^{2+}/calmodulin-dependent protein kinase II in the *Drosophila* brain using a specific monoclonal antibody. *Brain Res* 974:99–116.
40. Ashraf SI, McLoon AL, Sclarsic SM, Kunes S (2006) Synaptic protein synthesis associated with memory is regulated by the RISC pathway in *Drosophila*. *Cell* 124:191–205.
41. Krashes MJ, Keene AC, Leung B, Armstrong JD, Waddell S (2007) Sequential use of mushroom body neuron subsets during *Drosophila* odor memory processing. *Neuron* 53:103–115.
42. McGuire SE, Le PT, Davis RL (2001) The role of *Drosophila* mushroom body signaling in olfactory memory. *Science* 293:1330–1333.
43. Chen X, *et al.* (2005) Mass of the postsynaptic density and enumeration of three key molecules. *Proc Natl Acad Sci USA* 102:11551–11556.
44. Sugiyama Y, Kawabata I, Sobue K, Okabe S (2005) Determination of absolute protein numbers in single synapses by a GFP-based calibration technique. *Nat Methods* 2:677–684.
45. Giepmans BN, Deerinck TJ, Smarr BL, Jones YZ, Ellisman MH (2005) Correlated light and electron microscopic imaging of multiple endogenous proteins using Quantum dots. *Nat Methods* 2:743–749.
46. Wang W, *et al.* (2004) Conserved C-terminal threonine of hepatitis C virus NS3 regulates autoproteolysis and prevents product inhibition. *J Virol* 78:700–709.
47. Taremi SS, *et al.* (1998) Construction, expression, and characterization of a novel fully activated recombinant single-chain hepatitis C virus protease. *Protein Sci* 7:2143–2149.
48. Tong X, *et al.* (2006) Identification and analysis of fitness of resistance mutations against the HCV protease inhibitor SCH 503034. *Antiviral Res* 70:28–38.
49. Yao N, *et al.* (1997) Structure of the hepatitis C virus RNA helicase domain. *Nat Struct Biol* 4:463–467.
50. Steinkuhler C, *et al.* (1998) Product inhibition of the hepatitis C virus NS3 protease. *Biochemistry* 37:8899–8905.
51. Zhang R, *et al.* (1997) Probing the substrate specificity of hepatitis C virus NS3 serine protease by using synthetic peptides. *J Virol* 71:6208–6213.

Supporting Information

Lin et al. 10.1073/pnas.0803060105

SI Materials and Methods

Neuronal Experiments. Hippocampal neurons were dissected from postnatal day 0 or 1 rat pups and cultured on poly-D-lysine-coated plastic plates in Neurobasal medium supplemented with B27 and glutamine. For immunoblotting experiments, neurons were transfected before plating using the Amaxa Nucleofector protocol. For other experiments, neurons were transfected at 7–10 days *in vitro* (DIV) by the calcium phosphate method.

For time lapse imaging, we chose 14–21 DIV neurons with pyramidal morphology expressing PSD-95-GFP-TimeSTAMPa-HA with dim GFP fluorescence. These were imaged for GFP by epifluorescence on a Zeiss Axiovert 200M with a temperature control chamber at 37°C and a 100× oil objective in HBSS supplemented with B27 and 10 μM BILN-2061. For each position and time point, a stack of 20 images spaced 0.5 μm apart through the neurons was acquired. After fixation with 4% paraformaldehyde for 10 min, neurons were stained for HA and synapsin by standard protocols and then imaged again for GFP, HA, and synapsin. Image stacks were cropped to remove sections lost to focal drift and flattened into single maximum projection images for analysis.

For synaptic density quantification in neurons transfected with various fusions of PSD-95-GFP to NS3, maximum intensity projections of stacks of 20 images spaced 0.5 μm apart of 14 DIV neurons at 7 days posttransfection (DPT) were acquired of GFP fluorescence and synapsin immunofluorescence in a blinded manner. In ImageJ software, a 60-μm-long segment of the primary dendrite beginning 30 μm from the cell body was traced in the GFP channel and then dilated by 1 μm and used as a positive mask for the synapsin channel. Synapsin staining within the mask was isolated by using the automatic threshold function. Synaptic density was defined as the area covered by synapsin staining, as calculated by using the analyze particles function, divided by the mask area.

For EosFP photoconversion experiments, because photoconversion is most effective at pH <7, neurons expressing proteins fused to tdEosFP were moved into HBSS (pH 6.9) supplemented with B27 as a source of antioxidants. Focal photoconversion was performed in a temperature control chamber at 37°C on an inverted microscope using illumination from a xenon arc lamp passing through a 420/20-nm bandpass filter, a stopped-down diaphragm, and a 100× oil objective. Under these conditions, red fluorescence increases to 4-fold over beginning levels by 1.5 min of illumination, remains constant over the next 1.5 min, then falls, presumably because of photobleaching. After undergoing rapid and variable photoactivation, green fluorescence drops to 0.5× of maximal values by 1.5 min, then to 0.35× by 3 min. Further illumination was associated with blebbing of illuminated neurites. To minimize phototoxicity and maximize red fluorescence marking locally converted protein, we therefore performed photoconversion for 3 min. Global photoconversion was performed on a solar simulator with a xenon arc lamp passing through a 420/40 bandpass filter for 40 min, resulting in a 9-fold increase in red fluorescence and a final green fluorescence 10% of beginning values. After photoconversion, neurons were returned to conditioned Neurobasal medium with B27 and maintained at 37°C and 5% CO_2 and imaged in HBSS at various times afterward.

Fly Experiments. Homozyous transformed lines were established from single progeny of embryos injected with pUAST-HSV-TimeSTAMPt-HA-dCaMKII or pUAST-HSV-TimeSTAMPa-HA-dCaMKII. Homozygotes showed no behavioral or fertility phenotypes, and no loss of P-elements or transposition to other chromosomes were observed in balanced lines. Homozygous adults had smooth eyes, and brains were normal in size. Male homozygotes with third-chromosome insertions were crossed to elav-GAL4;UAS-tubulin-GFP;+ females, and the male elav-GAL4/Y;UAS-tubulin-GFP/+;HSV-TimeSTAMP-HA-dCaMKII/+ progeny were used for experiments between 1 and 2 days after eclosion.

For experiments involving HSV-TimeSTAMPt-HA-dCaMKII, flies were anesthetized by carbon dioxide, then a hole was punctured in the medial ocellus region using a glass micropipette with a 10-μm bore, and a 25-nl drop of 2 mM BILN-2061 in 20% DMSO 5% Cremophor EL in HBSS was placed over the region. The drug solution was observed to be absorbed within 2 min, then flies were returned to food vials with a wetted plug and allowed to recover. After recovery, flies were observed to feed, fly, and engage in courtship behavior. For HSV-TimeSTAMPa-HA-dCaMKII, flies were starved for 12 h with only water and then placed in a vial with an emulsion of 30% (wt/vol) yeast, 30% (vol/vol) glycerol, 30% (vol/vol) water, 5% green food coloring, 5% dimethylformamide, and 500 μM BILN-2061. Most flies were observed to ingest the food coloring within 15 min. For analysis, flies were immersed and rapidly decapitated in fixative (HBSS with 4% paraformaldehyde and 0.2% Triton X-100), and brains were dissected and incubated in fixative for a total of 40 min at room temperature. Brains were processed for immunocytochemistry by standard methods and imaged on a Zeiss LSM510 or LSM5Live confocal microscope.

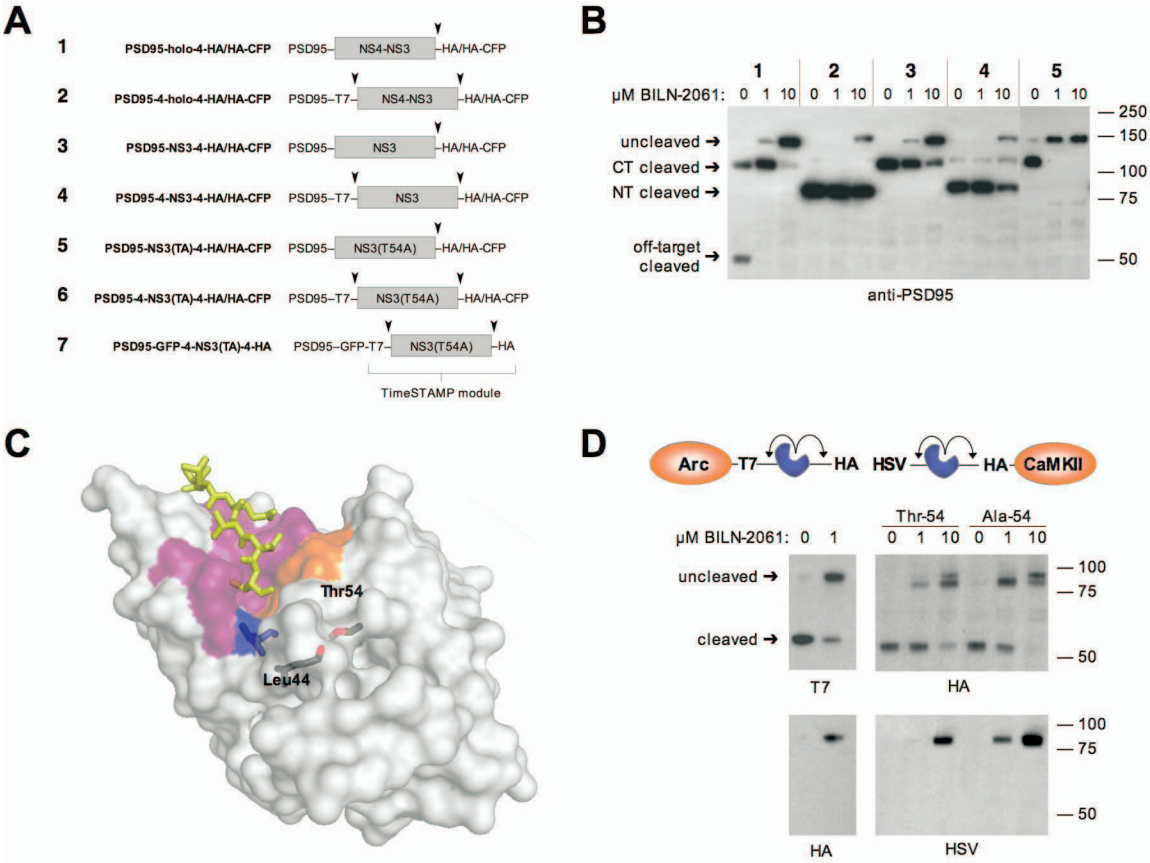

Fig. S1. Optimization of TimeSTAMP. (*A*) Organization of fusion proteins used in *B* and Fig. S2C. (*B*) Cyan fluorescent protein-containing constructs 1–5 from *A* were expressed in HEK293 cells in 0, 1 μM, or 10 μM BILN-2061, and cleavage of the constructs was assayed by immunoblotting. (*C*) The T54A reduced activity mutation is unlikely to affect substrate or BILN-2061 binding. Substrate-bound NS3 was rendered based on coordinates from Protein Data Base ID code 1CU1. A P1 to P6 substrate is shown as yellow sticks. The BILN-2061 contact surface, the catalytic triad, and the oxyanion hole are purple, orange, and blue, respectively. The backbone atoms of the oxyanion hole residues are shown as blue sticks. The side chain and backbone carbonyl of Leu-44 and the side chain of Thr-54 are shown as sticks with carbon atoms in black, oxygen in red, and hydrogen in white. (*D*) The TimeSTAMP module functions at either the N terminus or C terminus. HEK293 cells expressing Arc-TimeSTAMPa-HA at 37°C (*Left*) or HSV-TimeSTAMPt-HA-dCaMKII or HSV-TimeSTAMPa-HA-dCaMKII at 25°C (*Right*) in the continual absence or presence of BILN-2061 were analyzed by immunoblotting.

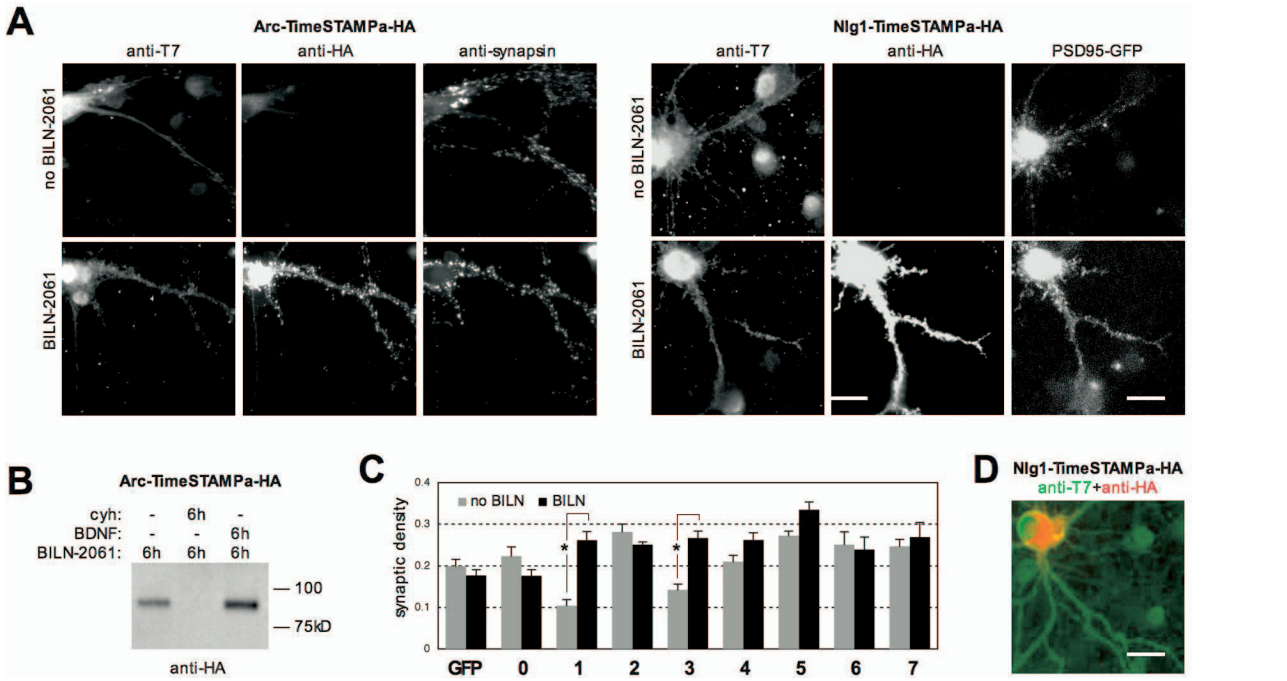

Fig. S2. TimeSTAMP is generalizable and functions in neurons without toxicity. (*A*) Neurons were transfected at 9 DIV with fusions of Arc (*Left*) or Neuroligin1 (Nlg1; *Right*) to TimeSTAMPa-HA and grown in the absence or presence of BILN-2061 for 3 days. To mark synapses, Nlg1-TimeSTAMPa-HA-expressing neurons were cotransfected with PSD-95-GFP, and Arc-TimeSTAMPt-HA-expressing neurons were stained for synapsin. T7 is a constitutive tag located N-terminal to the left cleavage site, and HA is drug-dependent. Anti-T7 cross-reactivity to the nucleus has been previously observed in various cell types. (*B*) TimeSTAMP detects stimulus-dependent new protein synthesis in neurons. Neurons were transfected by Amaxa nucleofection at 0 DIV with Arc-TimeSTAMPa-HA and analyzed at 7 DIV. HA-tagged Arc appearing after incubation in 10 μM BILN for 6 h was blocked with simultaneous cycloheximide (cyh; 50 μg/ml) treatment and increased with simultaneous BDNF stimulation. (*C*) Quantification of synaptic density in cells transfected with the PSD-95 fusions shown in *A*. Each condition contained 5 neurons scored blinded. Differences were significant by ANOVA ($P = 0.0057$). Only permanent fusions of wild-type NS3 show significantly lower synaptic density in the absence of inhibitor ($P < 0.05$ on pairwise *t* tests, asterisks). Data represent mean $\pm$ SEM. (*D*) Nlg1-TimeSTAMPa-HA reveals distribution of newly synthesized Nlg1 after 6 h. (Scale bars, 20 μm.)

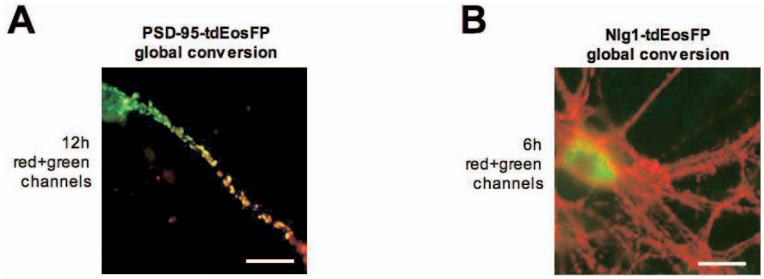

Fig. S3. Validation of protein movements using the photoconvertible protein tdEosFP. (*A*) After PSD-95-tdEosFP in 12 DIV neurons was photoconverted globally to red, new green protein was observed in a gradient from the cell body 12 h later, confirming results obtained by TimeSTAMP. (*B*) Similarly, 6 h after photoconversion, new Nlg1-tdEosFP protein was observed in the soma in a perinuclear distribution consistent with movement through the secretory pathway. (Scale bars, 20 μm.)

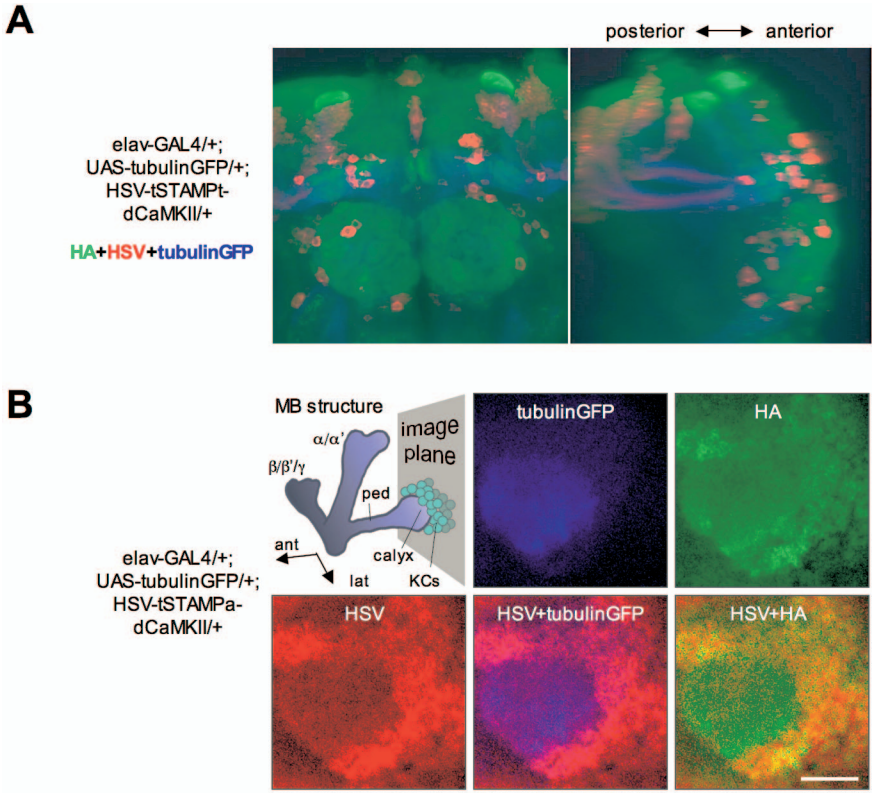

Fig. S4. TimeSTAMP reveals tissue and subcellular locations of newly synthesized dCaMKII. (*A*) A three-dimensional map of 6-h fractional new dCaMKII was constructed in flies expressing HSV-TimeSTAMPt-HA-dCAMKII. Anti-HSV labels new dCaMKII, and anti-HA labels total dCaMKII. Front and side projections of confocal sections spaced 2 μm apart are shown. (*B*) HA staining of flies expressing HSV-TimeSTAMPa-HA-dCaMKII shows total dCaMKII in Kenyon cell bodies and within the calyx, which is enriched in tubulin-GFP. HSV staining reveals recently synthesized dCaMKII is enriched in the cell bodies. (*Upper Left*) Diagram of the left mushroom bodies. ped, peduncle; KCs, Kenyon cell bodies; ant, anterior; lat, lateral. (Scale bar, 10 μm.)